Shear-induced sedimentation in yield stress fluids

Guillaume Ovarlez, François Bertrand, Philippe Coussot, Xavier Chateau

Shear-induced sedimentation in yield stress fluids

Guillaume Ovarlez*, François Bertrand, Philippe Coussot, Xavier Chateau

Université Paris-Est, Laboratoire Navier (UMR CNRS 8205), Champs-sur-Marne, France

Abstract

Stability of coarse particles against gravity is an important issue in dense suspensions (fresh concrete, foodstuff, etc.). On the one hand, it is known that they are stable at rest when the interstitial paste has a high enough yield stress; on the other hand, it is not yet possible to predict if a given material will remain homogeneous during a flow. Using MRI techniques, we study the time evolution of the particle volume fraction during the flows in a Couette geometry of model density-mismatched suspensions of noncolloidal particles in yield stress fluids. We observe that shear induces sedimentation of the particles in all systems, which are stable at rest. The sedimentation velocity is observed to increase with increasing shear rate and particle diameter, and to decrease with increasing yield stress of the interstitial fluid. At low shear rate ('plastic regime'), we show that this phenomenon can be modelled by considering that the interstitial fluid behaves like a viscous fluid – of viscosity equal to the apparent viscosity of the sheared fluid – in the direction orthogonal to shear. The behavior at higher shear rates, when viscous effects start to be important, is also discussed. We finally study the dependence of the sedimentation velocity on the particle volume fraction, and show that its modelling requires estimating the local shear rate in the interstitial fluid.

Keywords: Sedimentation; Yield stress fluid; Suspension; MRI

1. Introduction

Dense suspensions arising in industrial processes (concrete casting, drilling muds, foodstuff transport...) and natural phenomena (debris-flows, lava flows...) often contain coarse particles that tend to settle as they are denser than the average system density. This is a critical problem: if settling occurs, the materials may

*corresponding author: guillaume.ovarlez@ifsttar.fr

lose their homogeneity, which can strongly affect their mechanical properties. In slow flows, when the solid particles are immersed in a fluid, it is considered that the settling properties of suspended particles are not significantly affected by the material flow, and the sedimentation velocity is usually computed from the balance of gravity and drag forces. In order to avoid or slow down sedimentation, the only practical solution consists in inducing a sufficient agitation to the system which will induce some lift or dispersion forces to the particles. This principle is typically used in fluidization process, in which a vertical flow of the interstitial fluid induces a drag force counterbalancing gravity force. For horizontal flows in conduits one may also rely on turbulence effects [1, 2] or on viscous resuspension [3, 4].

For many materials, the situation is different: the denser particles do not settle at rest because they are embedded in a yield stress fluid which is able to maintain the particles in their position. This situation is typically encountered with mortars or fresh concrete [5, 6] which are made of particles (sand or gravel) of density around 2.5 mixed with a cement-water paste of density around 1.5. This is the same for toothpastes which contain silica particles of density 2.5 suspended in a paste of density close to 1. Basically, the net gravity force exerted on particles of diameter d suspended in a yield stress fluid of yield stress τ_y is counterbalanced by the elastic force exerted by the interstitial material as long as $\Delta\rho g d \lesssim \tau_y$, where $\Delta\rho$ is the density difference between the fluid and the particles. More precisely, it has been shown theoretically [7] and experimentally [8] that a single sphere in an infinite yield stress fluid does not settle as long as

$$\frac{\tau_y}{\Delta\rho g d} \geq \frac{1}{21} \tag{1}$$

However, it is usually observed that a significant sedimentation can occur in such materials when they are handled [9]. Thus the question we address here is whether the above stability criterion still holds for particles in a flowing paste. Whereas stability and sedimentation at rest have been thoroughly studied in the literature [10], these issues have been poorly addressed in flowing yield stress fluids. The sedimentation of a single particle in non-Newtonian fluids sheared in a Couette geometry has been studied by Gheissary & vandenBrule [11]. For all materials, they attempt to model the sedimentation velocity of the particle, as a function of the applied shear rate $\dot{\gamma}$, by the Stokes velocity $V = (1/18)\Delta\rho g d^2/\eta_0$ in a viscous fluid of viscosity η_0 equal to the apparent viscosity $\eta(\dot{\gamma})$ of the sheared fluid. For three different shear-thinning fluids, they then find that the sedimentation velocity is significantly lower than expected. This suggests that the apparent

viscosity in the direction of sedimentation is higher than the apparent viscosity experienced in the Couette flow, a phenomenon they attribute to the anisotropic character of the studied materials. The case of a single particle in a Carbopol gel is also reported; it is worth noting that the particle is not stable at rest. In this case only, good agreement is found between the measured and predicted sedimentation velocity.

To our knowledge, sedimentation during a yield stress fluid flow of particles stable at rest has only been previously studied by Merkak *et al.* [12], in pipe flows. Merkak *et al.* [12] have observed that particles settle in the sheared fluid in some cases only; they have rationalized their observations by introducing a new criterion: they claim that particles do not settle in the sheared yield stress fluid if

$$\frac{\tau_y}{\Delta\rho g d} \gtrsim 3 \tag{2}$$

In the cases where sedimentation is observed, no characterization of the observed sedimentation velocity is reported.

In this paper, we address the question of the impact of a flow on the possible settling of coarse particles suspended in a yield stress fluid. Model density-mismatched suspensions of monodisperse particles are designed to be stable at rest. We focus on a well-controlled situation: the material is sheared in a coaxial cylinders (Couette) geometry, which imposes shear in the plane perpendicular to gravity; the sedimentation flow is thus decoupled from the shear flow (Fig. 1). We use Magnetic Resonance Imaging (MRI) as a noninvasive technique to study the time evolution of the particle volume fraction during shear. We first study the situation of low solid fractions for which we expect that particle interactions are small. Then we study the case of higher solid fractions, for which collective effects are known to play a significant role for particles settling in a simple viscous fluid [13, 14]. We study the sedimentation velocity as a function of the material properties, of the particle volume fraction, and of the characteristics of shear. We then propose a model to account for the observed features.

2. Materials and methods

2.1. Materials

Most model suspensions we study are suspensions of monodisperse glass beads in concentrated emulsions; the particle volume fraction ϕ is varied between 5% and 40%. We use spherical glass particles of four different diameters (145, 275,

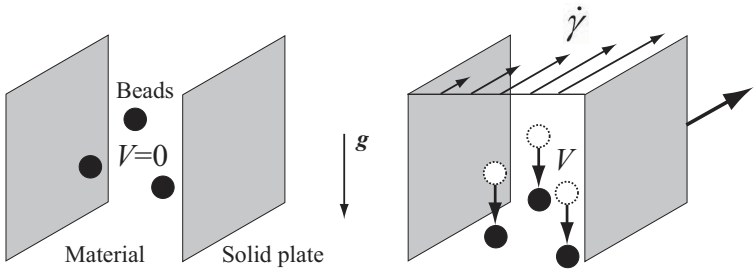

Figure 1: Sketch of the experiment.

375, and 405 μm $\pm 7\%$). The emulsions are prepared by dispersing a 100 g/l water solution of $CaCl_2$ in a solution of Span 80 emulsifier (7%) in dodecane oil at 6000 rpm with a Silverson L4RT mixer. The average droplet size is 1 μm; the emulsions are then viewed by the particles as continuous media [15]. In order to study materials of various rheological properties, we have varied the droplet concentration between 72 and 85%. We have also studied a 5% suspension of 405 μm glass beads in a Carbopol gel. The gel is obtained by dispersing Carbopol 980 (from Noveon) at a 0.3% concentration in water at 1000 rpm during 30 min; it is then neutralized with NaOH at pH=7 and stirred for an entire day to ensure homogeneity of the material.

We finally obtain 8 different materials, the properties of which are displayed in Tab. 1. Due to the specificity of our setup, which implies to use 1 liter of material per experiment and does not allow performing many experiments during a same period, we could not ensure the reproducibility of the emulsion properties, which explains the variety of the materials. We were thus able to vary the particle diameter in exactly the same material only once.

The density of the glass particles is 2.5 whereas the density of all the studied yield stress fluids is of order 1. Gravity thus tends to induce sedimentation of the particles. However, all systems are designed to be stable at rest: their yield number $Y = \frac{\tau_y}{\Delta\rho g d}$ complies with Eq. 1 (see Tab. 1), which ensures that elastic forces exerted by the yield stress fluid at rest are able to counterbalance the net gravity force.

2.2. Rheometry

The yield stress fluid rheological properties are characterized in a sandblasted 2 $^\circ$ cone-and-plate geometry of 40 mm diameter, with a Bohlin C-VOR 200 rheometer. The material is presheared at a 50 s^{-1} shear rate during 60 s. The shear rate $\dot{\gamma}$

τ_y (Pa)	η_{HB} (Pa.s^n)	n	d (μm)	ϕ (%)	$Y = \frac{\tau_y}{\Delta\rho g d}$
concentrated emulsions					
8.5	3.6	0.44	275	5	2.1
16.5	3.8	0.5	375	5 to 40	2.9
15.1	3.25	0.5	275	5; 10	3.7
21.4	4.25	0.5	405	5	3.6
25	10	0.4	145	5	12.1
33.2	5.0	0.5	275	5	8.2
33.2	5.0	0.5	405	5	5.6
Carbopol gel					
27.5	10.1	0.35	405	5	4.7

Table 1: Properties of the studied materials: yield stress τ_y, consistency η_{HB} and index n of the yield stress fluids (all material flow curves were fitted to a Herschel-Bulkley law $\tau = \tau_y + \eta_{HB}\dot{\gamma}^n$); glass bead diameter d; particle volume fraction ϕ. The yield number $Y = \frac{\tau_y}{\Delta\rho g d}$ used in stability criteria (Eqs. 1 and 2) is also provided.

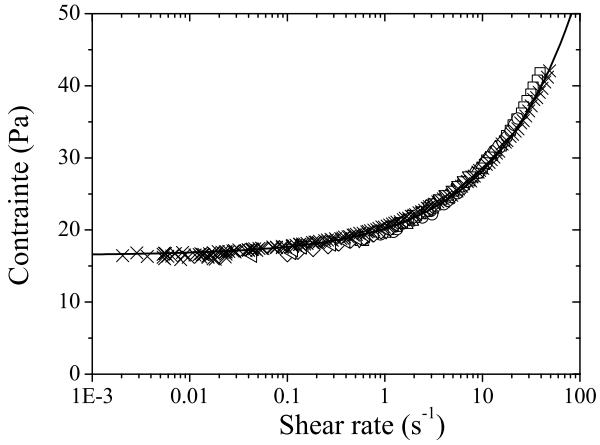

Figure 2: Constitutive law $\tau(\dot{\gamma})$ of a concentrated emulsion obtained (i) from macroscopic measurements in a cone-and-plate geometry (crosses) and (ii) from local MRI measurements in a Couette geometry (empty symbols; different symbols correspond to different inner cylinder rotational velocity). The solid line is a Herschel-Bulkley fit to the macroscopic data $\tau = \tau_y + \eta_{HB}\dot{\gamma}^n$ with $\tau_y = 16.5$ Pa, η_{HB}=3.8 Pa s$^{0.5}$, and $n = 0.5$.

is then ramped-down from 50 s^{-1} to 0.001 s^{-1} (logarithmic ramp, 30 s/decade of shear rate), and shear stress vs. shear rate data $\tau(\dot{\gamma})$ are recorded during the ramp. We checked that the materials we study are simple yield stress fluids which do not display thixotropy, in agreement with previous investigations [16, 17]. $\tau(\dot{\gamma})$ data obtained in one of the concentrated emulsions are displayed in Fig. 2. All material behaviors are well fitted to a Herschel-Bulkley behavior $\tau(\dot{\gamma}) = \tau_y + \eta_{HB}\dot{\gamma}^n$ (an example is shown in Fig. 2); the values of the rheological parameters (τ_y, η_{HB}, n) measured on all the studied materials are displayed in Tab. 1.

2.3. Sedimentation experiments

The suspensions are loaded in a Couette geometry, the dimensions of which are: inner cylinder radius, $R_i = 4.1$ cm; outer cylinder radius, $R_o = 6$ cm; height of sheared fluid, $H = 11$ cm. Both cylinders are covered with sandpaper to avoid wall slip. Shear is induced by the rotation of the inner cylinder at controlled rotational velocity Ω. The Couette rheometer is inserted in a Magnetic Resonance Imaging (MRI) setup described in [18].

Azimuthal velocity profiles $v_\theta(r)$ are measured using MRI techniques [18, 19]; an example is shown in Fig. 3a. The local shear rate $\dot{\gamma}(r)$ at a radius r in the gap can then be deduced from $v_\theta(r)$ as $\dot{\gamma}(r) = v_\theta(r)/r - \partial_r v_\theta(r)$; the derivative $\partial_x f$ with respect to coordinate x of experimental data $f(x_i)$ measured at regularly spaced positions x_i was here computed as: $\partial_x f(x_i) = [f(x_{i+1}) - f(x_{i-1})]/[x_{i+1} - x_{i-1}]$.

When the material is homogeneous along the vertical direction, the local shear stress $\tau(r)$ within the gap is obtained from torque T measurements as $\tau(r) = T/(2\pi r^2 H)$. Local data $\big(\tau(r,\Omega), \dot{\gamma}(r,\Omega)\big)$ measured at various r and various Ω can finally be combined to obtain the constitutive law $\tau(\dot{\gamma})$ consistent with the observed flows (more details about this reconstruction technique can be found in [16]). Local $\tau(\dot{\gamma})$ data measured with this method in a (pure) concentrated emulsion are displayed in Fig. 2. We observe that there is good agreement between these local measurements and the macroscopic measurements obtained in the cone-and-plate geometry. This shows the ability of the macroscopic measurements to account for the steady-state flow behavior of the material in our experiments in a wide-gap Couette geometry.

To investigate shear-induced sedimentation, we study the time evolution of the r-averaged vertical profile $\phi(z)$ of the particle volume fraction in the suspensions for rotational velocity Ω of the inner cylinder ranging between 5 and 100 rpm. The particle volume fraction is obtained both in radial and vertical directions from density imaging with an accuracy of 0.2% [20]. The use of a wide gap allows us

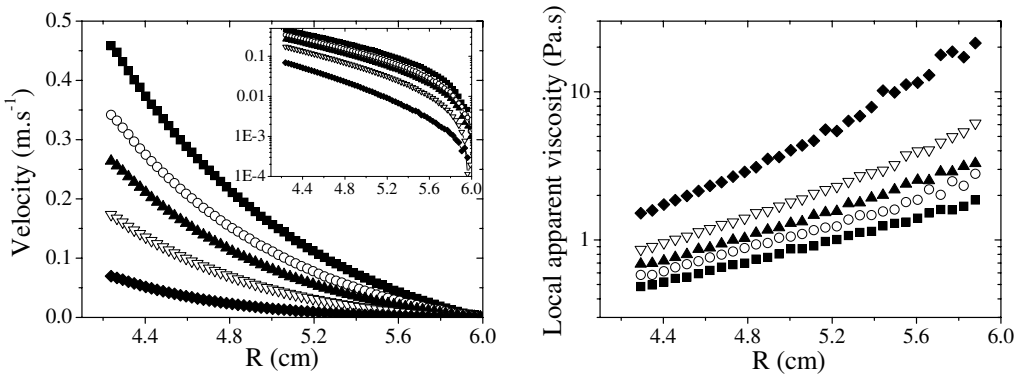

Figure 3: (a) Local velocity $v_\theta(r)$ in a 5% suspension of 275 μm glass beads in a concentrated emulsion of yield stress $\tau_y = 8.5$ Pa sheared in the gap of a Couette geometry, for various rotational velocities Ω of the inner cylinder (squares: 130 rpm, empty circles: 100 rpm, up triangles: 75 rpm, empty down triangles: 50 rpm, diamonds: 20 rpm). The inset is a semi-log plot of the same data. (b) Local apparent viscosity $\eta[\dot\gamma(r)]$ deduced from the velocity profiles of Fig.3a.

to study large particles. However, it results in unavoidable stress heterogeneity, as the shear stress distribution is $\tau(r) = \tau(R_i)R_i^2/r^2$. We thus have to be careful about shear localization in the experiments [21]; unless otherwise noted, all Ω were high enough to ensure that the whole gap is sheared (see e.g. Fig. 3a inset). Nevertheless, due to the nonlinear behavior of the studied materials, the shear rate and apparent viscosity distributions are strongly heterogeneous. To illustrate this point, we have computed the local apparent viscosity $\eta[\dot\gamma(r)]$ of the material in the gap of the geometry from the interstitial yield stress fluid behavior as $\eta[\dot\gamma(r)] = \left(\tau_y + \eta_{HB}\dot\gamma(r)^n\right)/\dot\gamma(r)$ and have plotted these values in Fig. 3b in the case of the emulsion of Fig. 3a. It is observed that, depending on the material and on the boundary conditions, the shear rate varies by a typical factor of order 10 from the inner to the outer cylinder, leading to spatial evolution of the apparent viscosity by a factor of 5.

This heterogeneity is negligible at the particle scale but important at the suspension scale, and it may have an impact on the spatial characteristics of sedimentation. This issue is discussed in Sec. 3.1 and in the Appendix A. To minimize the possible impact of this heterogeneity, we have measured the vertical concentration profiles $\phi(z)$ only in a 9 mm thick zone in the gap (from $r = 4.4$ cm to $r = 5.3$ cm); in this region, the apparent viscosity of the material is observed

to vary typically by a factor of 2. In the following, the results are presented as a function of the spatial average $\bar{\dot{\gamma}}$ of $\dot{\gamma}(r)$ in the measurement window. In the experiments, $\bar{\dot{\gamma}}$ was varied between 3 and 25 s^{-1}.

All suspensions are stable at rest: the material yield stress is more than 40 times higher than that fixed by the stability criterion Eq. 1 (see Tab. 1). We have checked that the volume fraction profiles remain indeed homogeneous at rest during 24 h (Fig. 4). Moreover, for 5 of the materials, the yield stress of the interstitial fluid is higher (up to 4 times) than that fixed by the stability criterion under shear Eq. 2 proposed by Merkak *et al.* [12], whereas it is lower for 2 of the materials.

In the following, in order to minimize the role of the particle interactions, we first focus on the behavior of semi-dilute suspensions of particle volume fraction $\phi = 5\%$ (Sec. 3). We then study the impact of a change in ϕ (Sec. 4).

3. Shear-induced sedimentation in a semi-dilute suspension

3.1. Volume fraction profiles

In Fig. 4, we show vertical volume fraction profiles observed at rest and during shear in one of the studied suspensions of particle volume fraction $\phi = 5\%$. The same features are observed in all the systems we have studied.

At rest, the particles appear to remain indefinitely in their initial position: there is no observable difference between the vertical concentration profiles measured after loading and after a 24 h rest. Whereas the particles are stable at rest, we observe that there is sedimentation when the material is sheared. The sedimentation profiles measured during shear show classical features of sedimentation in Newtonian fluids [2]: the upper part is at a 0% concentration, the middle part remains at the initial 5% concentration, and the particles tend to accumulate at the bottom of the cup, in the dead zone below the inner cylinder end. The transition zone between the 0% and the 5% regions is rather narrow (with a typical thickness of 6mm), and defines a sedimentation front that moves continuously towards the bottom as the flow duration increases.

We do not observe any significant broadening of the sedimentation front in time. This implies that, although the shear rate distribution is heterogeneous in the gap (we recall that $\dot{\gamma}(r)$ varies typically by a factor of 4 in the measurement zone), there is no significant spatial heterogeneity of the sedimentation velocity, which suggests that collective effects are at play. This issue is discussed in more detail in the Appendix A. In the following, we will thus assume that it is sufficient to consider the average shear rate $\bar{\dot{\gamma}}$ to describe shear-induced sedimentation.

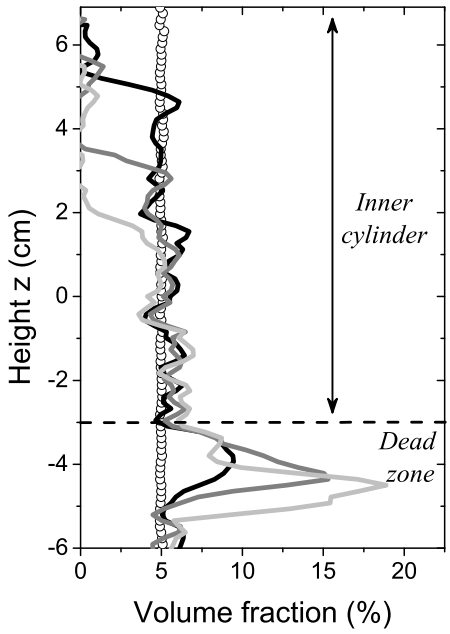

Figure 4: Vertical volume fraction profiles observed in the gap of a Couette geometry in a 5% suspension of 275 μm glass beads in a concentrated emulsion of yield stress $\tau_y = 8.5$ Pa, after a 24 h rest (empty circles) and after 15 min (black line), 30 min (dark grey line) and 45 min (light grey line) of shear at $\bar{\dot{\gamma}} = 4$ s^{-1}.

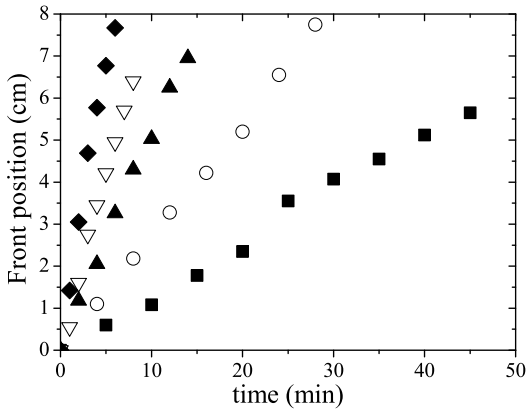

Figure 5: Position of the sedimentation front as a function of the time of shear, for a 5% suspension of 275 μm glass beads in a concentrated emulsion of 8.5 Pa yield stress, for various shear rates: 4 s^{-1} (squares), 8.8 s^{-1} (empty circles), 14 s^{-1} (up triangles), 18.6 s^{-1} (empty down triangles) and 25 s^{-1} (diamonds).

We observe that the sedimentation front moves linearly in time (Fig. 5). We thus extract the sedimentation velocity V of the suspension from a linear fit to the front position vs. time data.

3.2. Conditions of stability

The stability at rest of the systems we have studied is consistent with Eq. 1 (see the values of their yield number Y in Tab. 1). However, our observations contrast with previous observations [12]: we find that shear induces sedimentation in all of our systems, at any imposed shear rate. It thus seems that the proposed stability criterion Eq. 2 is not correct (most of our systems verify Eq. 2, see Tab. 1); from our observations, the possibility of stability under shear is actually doubtful. The absence of observable sedimentation in some of the Merkak *et al.* [12] experiments is likely due to the fact that, as shown below in Secs. 3.3 and 3.4, the sedimentation velocity can be very small at high material yield stress and small particle diameter.

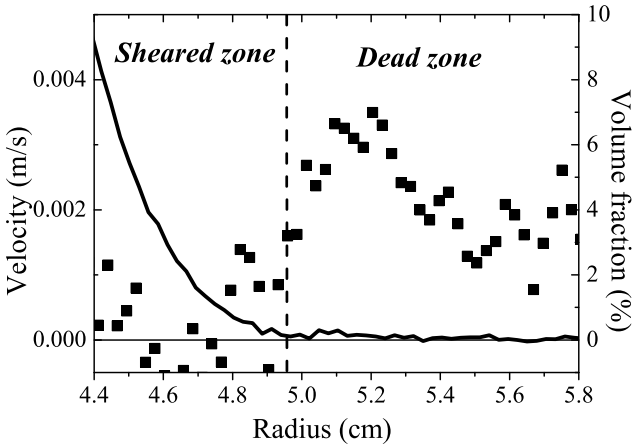

Figure 6: Velocity profile (line, left axis) and radial volume fraction profile (squares, right axis) observed in the gap of a Couette geometry in a 5% suspension of 405 μm glass beads in a concentrated emulsion of yield stress $\tau_y = 21.4$ Pa, after 24 h of shear at $\Omega = 4$ rpm.

To illustrate further the role of shear on sedimentation, we have performed an experiment in which flow is localized (Fig. 6), by applying a low rotational velocity $\Omega = 4$ rpm to the inner cylinder on one of the systems. In these conditions, the material is sheared from the inner cylinder to the middle of the gap (at $R_c \simeq$ 4.95 cm), and at rest from R_c to the outer cylinder; the average shear rate in the

sheared region is of the order of 1 s^{-1}. We recall that shear localization is here due to the stress heterogeneity, as the local shear stress value is $\tau(r) = \tau(R_i)R_i^2/r^2$, which is equal to the yield stress of the material τ_y at the interface R_c between the sheared and the unsheared material. We have sheared the material during 24 h to ensure that all sedimentation has time to occur if it has to. We have measured the radial volume fraction profile $\phi(r)$ in the gap of the geometry after this 24 h shear (Fig. 6). It is observed that there are no more particles[1] in the sheared zone, and that the volume fraction in the unsheared zone is unchanged, consistently with the stability of the system at rest (see Fig.4). The interface between the zones at $\phi = 0\%$ and $\phi = 5\%$ exactly corresponds to the interface between the sheared and the dead zone. This clearly shows that sedimentation is induced as soon as the material is sheared, even when the applied stress is very close to the yield stress (i.e., near R_c, where the local shear rate is close to zero).

3.3. Sedimentation velocity

In order to better understand shear-induced sedimentation, we now compare the sedimentation velocities V observed in all systems under various conditions. Our observations can be summarized as follow:

- V increases with the applied shear rate $\bar{\dot{\gamma}}$ (Fig. 7)
- for a given particle diameter d, at a given $\bar{\dot{\gamma}}$, V is a decreasing function of the material yield stress τ_y (Fig. 7a).
- in a yield stress fluid of given rheological properties, V is an increasing function of the particle diameter d (Fig. 7b)

See also Fig. 8 where data obtained on all the studied materials are shown.

These results can be qualitatively understood: V is actually expected to decrease when the plastic to gravity stress ratio $Y = \frac{\tau_y}{\Delta\rho g d}$ increases. Moreover, the increase of V with $\bar{\dot{\gamma}}$ suggests that the settling particles are sensitive to the apparent viscosity $\eta(\bar{\dot{\gamma}}) = \tau(\bar{\dot{\gamma}})/\bar{\dot{\gamma}}$ of the sheared material, which decreases with $\bar{\dot{\gamma}}$ for all the studied materials.

[1] Note that the measurement fluctuations – of order 1% – are here much larger for radial profiles than for vertical profiles.

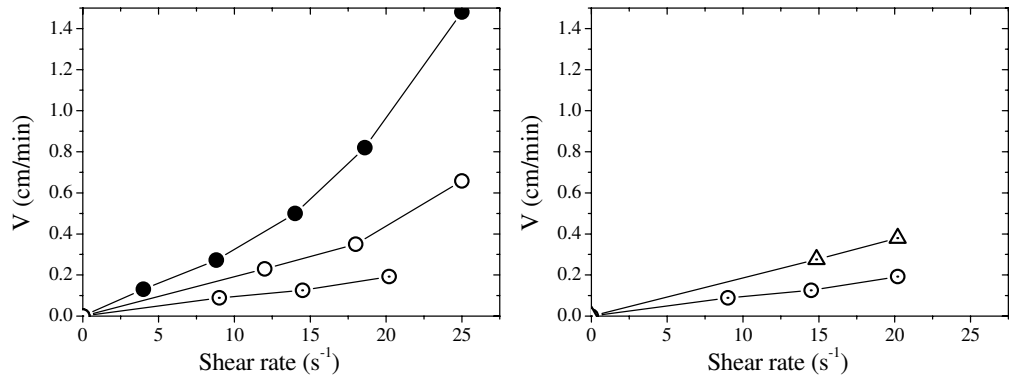

(a) (b)

Figure 7: (a) Sedimentation velocity V of 275 μm glass beads vs. shear rate $\bar{\dot{\gamma}}$ in three different concentrated emulsions, of yield stress 8.5 Pa (filled circles), 15 Pa (empty circles) and 33 Pa (dotted circles). (b) Sedimentation velocity V of 275 μm (dotted circles) and 405 μm (dotted triangles) glass beads vs. shear rate $\bar{\dot{\gamma}}$ in a concentrated emulsion of 33 Pa yield stress. The particle volume fraction of the suspensions is $\phi = 5\%$.

3.4. Theoretical analysis

In this section, we aim to better understand the phenomenon of shear-induced sedimentation, and to predict the value of the sedimentation velocity V as a function of the material and flow characteristics. We point out that the particle Reynolds number Re_p for both the shear flow ($\rho d^2\dot{\gamma}/\eta(\dot{\gamma})$) and the settling flow ($\rho dV/\eta(\dot{\gamma})$) is of order 10^{-3} or less in all experiments; our analysis is thus made in the Stokes regime. In the following, we first deal with the problem of the sedimentation of a single sphere of diameter d in the sheared yield stress fluid; we will comment on the volume fraction dependence of V below.

Shear-induced sedimentation involves a complex 3D flow of the yield stress fluid around the particle. We thus have to consider a tensorial form of the Herschel-Bulkley behavior; here we assume that the material behavior obeys its isotropic form [22, 23, 24]

$$\tau_{ij} = 2[(\tau_y + \eta_{HB}\dot{\gamma}^n)/\dot{\gamma}]d_{ij} \tag{3}$$

where τ_{ij} is the deviatoric stress tensor, d_{ij} is the strain rate tensor (i.e. the symmetric part of the velocity gradient), and the shear rate is $\dot{\gamma} = \sqrt{2d_{ij}d_{ij}}$. This form has been shown to be consistent with recent observations of complex yield stress fluid flows [24, 25].

When two orthogonal flows[2] are superimposed, it has been shown that, if the strain rate of one of the flows is much higher than that of the other flow, the flow resistance to the secondary flow is purely viscous (linear) and is characterized by an effective viscosity equal to the apparent viscosity $\eta(\dot{\gamma})$ of the main flow [24]. This can be understood for the isotropic Herschel-Bulkley law (Eq. 3): e.g, if we consider a main simple shear flow of strain rate $d_{r\theta}$ in a Couette geometry, the shear resistance τ_{rz} to a secondary orthogonal flow in the z direction, of strain rate d_{rz} such that $d_{rz} \ll d_{r\theta}$, is

$$\tau_{rz} \simeq 2[(\tau_y + \eta_{HB}(2d_{r\theta})^n)/2d_{r\theta}]\, d_{rz} = 2\eta(\dot{\gamma})\, d_{rz} \tag{4}$$

with $\dot{\gamma} \simeq 2d_{r\theta}$: the flow resistance to this secondary flow in the vertical direction is thus characterized by a viscous behavior of effective viscosity $\eta(\dot{\gamma}) = [(\tau_y + \eta_{HB}\dot{\gamma}^n)/\dot{\gamma}]$ fixed by the characteristics of the Couette flow only.

In all of our experiments, the settling flow can be considered as a secondary flow as compared to the shear flow. Indeed, its characteristic shear rate $\dot{\gamma}_s$ is of order V/d; this value is here 50 to 400 times lower than $\dot{\gamma} \simeq 2d_{r\theta}$. In these conditions, given the above remarks about the flow resistance to secondary flows, it is tempting to model the sedimentation velocity of a single sphere in the sheared yield stress fluid by the velocity V_{Stokes} of a sphere in a Newtonian medium of viscosity given by the apparent viscous resistance $\eta(\dot{\gamma}) = \tau(\dot{\gamma})/\dot{\gamma}$ to the shear flow (here, $\tau = \tau_{r\theta}$ and $\dot{\gamma} = 2d_{r\theta}$ characterize the shear flow induced by the rotation of the inner cylinder of the Couette cell):

$$V_{\text{Stokes}} = \alpha_S \frac{\Delta\rho g d^2}{\eta(\dot{\gamma})} \tag{5}$$

with $\alpha_S = 1/18$.

However, this preliminary analysis does not account for the complexity of flow around a sphere: it is based on *orthogonal* superimposed flows, which is not the case of the shear and sedimentation flows around a sphere. In this last case, one cannot simply describe the shear resistance to sedimentation as in Eq. 4, because the strain rate tensor field around the sphere is not the sum of two orthogonal tensor fields (i.e., $\boldsymbol{d}_f : \boldsymbol{d}_{\text{p}} \neq 0$ in Eq. B.8). Moreover, the contribution to the drag force of the normal stresses exerted on the particle also have to be properly taken into account in the analysis. In the Appendix B, a rigorous theoretical analysis

[2]We recall that two flows of strain rate tensors d^1_{ij} and d^2_{ij} are said to be orthogonal when $d^1_{ij}\, d^2_{ij} = 0$.

of the problem of shear-induced sedimentation is made, in the case where the sedimentation flow is a secondary flow (i.e., when $V/d \ll \dot{\gamma}$). It is shown that the scaling proposed in Eq. 5 remains valid in two limit cases, for low and high inverse Bingham number $Bi^{-1}= \eta_{HB}\dot{\gamma}^n/\tau_y$.
When $Bi^{-1}\ll 1$ ('plastic' flows), it is expected that:

$$V = \alpha_p \frac{\Delta\rho g d^2}{\tau_y/\dot{\gamma}} \tag{6}$$

When $Bi^{-1}\gg 1$ ('viscous' flows), it is expected that:

$$V = \alpha_v \frac{\Delta\rho g d^2}{\eta_{HB}\dot{\gamma}^{n-1}} \tag{7}$$

Note that the constants α_p and α_v are unknown and are *a priori* different, which means that Eq. 5 cannot be correct and that in a general case, $V \not\propto 1/\eta(\dot{\gamma})$. Nevertheless, as it gives the correct scaling predictions in both the 'plastic' and 'viscous' limits, we will compare our results to Eq. 5 in the following.

These last equations are expected to be valid for a single sphere only, a case we cannot study with our means of investigation. We recall that our first results concern here semi-dilute suspensions of volume fraction $\phi = 5\%$. For a suspension of monodisperse spheres of volume fraction ϕ, by analogy with viscous suspensions, we expect the sedimentation velocity $V(\phi)$ of the suspension to be equal to that of a single sphere multiplied by a decreasing function of ϕ only, the hindrance function $f(\phi)$, with $f(0) = 1$ [13, 14] (we will come back onto this point in Sec. 4).

3.5. Comparison experiment/theory

In order to test the above theoretical analysis, we show the data obtained in all materials in Fig. 8a, and we plot all the measured sedimentation velocities V rescaled by the velocity V_{Stokes} given by Eq. 5 in Fig. 8b. We recall that V/V_{Stokes} is expected to tend towards two different constant values at low and large inverse Bingham number $Bi^{-1}= \eta_{HB}\bar{\dot{\gamma}}^n/\tau_y$. V/V_{Stokes} is thus plotted here vs. Bi^{-1}.

For shear-induced sedimentation in the concentrated emulsions, we first observe that all the data fall onto a master curve $V/V_{\text{Stokes}} \simeq 1.4$ up to $Bi^{-1}\simeq 1$, in good agreement with the theory in the 'plastic' regime. It is worth noting that the parameters d^2, τ_y and $\bar{\dot{\gamma}}$ involved in the scaling of Eq. 5 were here varied independently by a factor of 8, 4 and 4, respectively.

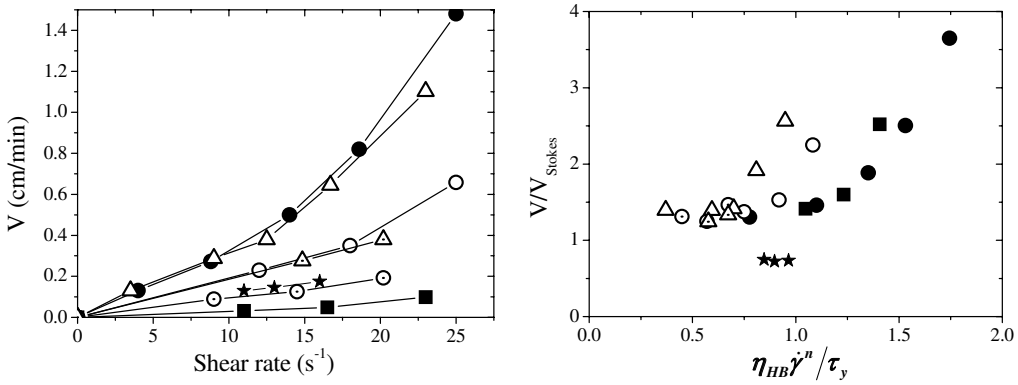

Figure 8: (a) Sedimentation velocity V of glass beads suspended at a 5% volume fraction in sheared yield stress fluids as a function of the applied shear rate $\bar{\dot{\gamma}}$, for various bead diameter d, various concentrated emulsions (filled squares: d=145 μm, $\tau_y = 25$ Pa; circles: d=275 μm, $\tau_y = 8.5$ Pa (filled), 15 Pa (empty), 33 Pa (dotted); triangles: d=405 μm, $\tau_y = 21.5$ Pa (empty), 33 Pa (dotted)) and a Carbopol gel (stars: d=405 μm, $\tau_y = 27.5$ Pa). (b) Same data rescaled by the velocity $V_{\text{Stokes}} = (\Delta\rho g d^2)/(18\eta)$ of a single sphere that would fall in a Newtonian medium of viscosity η equal to the apparent viscosity $\eta(\bar{\dot{\gamma}})$ of the pure sheared yield stress fluid; data are displayed vs. the inverse Bingham number $Bi^{-1} = \eta_{HB}\bar{\dot{\gamma}}^n/\tau_y$.

For higher values of Bi^{-1}, V/V_{Stokes} is then found to increase with Bi^{-1}; it can reach values that are up to 3 times higher than at low Bi^{-1} value. The existence of such a regime could be expected from the theory as V/V_{Stokes} *a priori* tends towards different values at low and high Bi^{-1}. However, we do not observe V/V_{Stokes} to tend towards a constant value when increasing Bi^{-1}, in contrast with what is expected in the 'viscous' regime. Nevertheless, it should be noted that the higher value of Bi^{-1} tested here was of order 1.8; further experiments at higher Bi^{-1} values would be needed to really test the theory in the 'viscous' regime. Data obtained here for $Bi^{-1} \gtrsim 1$ do not fall along a master curve, which means that the Bingham number should not be the only relevant parameter to consider to describe this intermediate regime.

For shear-induced sedimentation in the Carbopol gel, the important result is that the proposed scaling with the apparent viscosity of the sheared material $\eta(\dot{\gamma})$ seems to remain correct in the 'plastic' regime, as V/V_{Stokes} does not depend on $\bar{\dot{\gamma}}$ for $Bi^{-1} < 1$. Nevertheless, we now find a different value $V/V_{\text{Stokes}} \simeq 0.7$. It thus seems that shear-induced sedimentation is also sensitive to aspects of the material rheological behavior that we have not considered in the analysis. A possibility

is that normal stress differences play a role, since they can be large in sheared Carbopol gels [26], and since they are not taken into account in the expression of the Herschel-Bulkley law that we use.

For the sake of comparison with the properties of sedimentation in Newtonian fluids, we have performed sedimentation experiments with a 5% suspension of 275 μm glass beads in a Newtonian oil (viscosity 2.6 Pa.s), in several situations: (i) in the gap of the Couette cell at rest, (ii) in the gap of the Couette cell when the suspension is sheared, and (iii) in a large cylindrical container of 12 cm diameter and of 10 cm height. In the gap of the Couette cell, we have observed $V/V_{\text{Stokes}} \simeq 1.2$, both at rest and when the fluid is sheared (as expected from the linearity of the fluid behavior). In the cylindrical container, we have observed that $V/V_{\text{Stokes}} \simeq 0.7$ (note that $V/V_{\text{Stokes}} \simeq 0.8$ is expected at $\phi = 5\%$ in a Newtonian fluid in an 'infinite' geometry [13]). This shows that the characteristics of sedimentation in a Newtonian fluid are affected by the characteristics of the geometry we use[3]; it is also most probably the case for shear-induced sedimentation in a yield stress fluid. The value of V/V_{Stokes} we measure here would thus be difficult to compare to the results of analytic or numerical computations in plastic materials under homogeneous simple shear.

Note also that in Eq. 5 the sedimentation velocity is supposed to be set by the local value $\eta[\dot{\gamma}(r)]$ of the apparent viscosity of the sheared fluid, and thus to depend on the radial position r in the gap following $V(r) \propto 1/\eta[\dot{\gamma}(r)]$. In Fig. 3b we have shown that there are large $\eta[\dot{\gamma}(r)]$ variations in the gap: it varies typically by a factor of 5 in the whole gap and by a factor of 2 in the measurement zone, which should imply that, when averaging the sedimentation velocities in this zone, the sedimentation front corresponding to $\phi = 5\%$ in this region should move 2 times faster than the front corresponding to ϕ=0%. This is not the case experimentally as we have observed no broadening of the sedimentation front (Fig. 4), which suggests that collective effects are at play (see Appendix A for more details). This raises the question of the relevant value of $\eta[\dot{\gamma}(r)]$ to take into account in the theoretical analysis of the sedimentation velocity. Here we have no answer to this question: it could be the minimum or maximum value of $\eta[\dot{\gamma}(r)]$ in the gap, its average, etc. We have thus made an arbitrary choice by choosing $\eta(\bar{\dot{\gamma}})$. We

[3]This dependence could come, e.g., from the curvature of the geometry [27], from a small tilt angle [14], or from the limited size of the gap; we note in particular that the gap size is here of the order of the correlation length $\simeq 10d\phi^{-1/3}$ of the particle settling velocities [28], and that these fluctuations play a role in the backflow contribution to the suspension sedimentation velocity [28, 29].

checked that this choice is not crucial: e.g., putting the maximum or minimum value of $\eta[\dot{\gamma}(r)]$ in the gap in the analysis does not change the features observed experimentally (i.e., the existence of a plateau of V/V_{Stokes} at low Bi^{-1} and an increase of V/V_{Stokes} for $Bi^{-1} \gtrsim 1$). However, this choice affects the quantitative value of V/V_{Stokes}, which, again, would make it impossible to make a quantitative comparison to the results of analytic or numerical computations in plastic materials under homogeneous simple shear.

To conclude, we have shown that the sedimentation velocity of spherical particles at low solid fraction in a sheared yield stress fluid can be fairly predicted with Eq. 5 in the 'plastic' regime ($Bi^{-1} = \eta_{HB}\dot{\gamma}^n/\tau_y < 1$). The drag constant α seems to be close to that observed in Newtonian fluids, but its exact value cannot be directly derived from our experimental measurements as it depends on the characteristics of the geometry we use. The existence of a 'viscous' regime where the scaling of Eq. 5 should remain valid could not be tested with our systems; nevertheless, our results (the increase of V/V_{Stokes} with Bi^{-1} for $Bi^{-1} \gtrsim 1$) suggest that the drag constant α is significantly higher in this regime than in the 'plastic' regime. In the next section, we study the dependence of the sedimentation velocity on the solid fraction in the 'plastic' regime.

4. Dependence of the sedimentation velocity on the particle volume fraction

4.1. Observations

In a second stage, we have studied the impact of a change in the particle volume fraction ϕ on the sedimentation velocity. We have studied suspensions of 375 μm beads in a concentrated emulsion, with ϕ ranging from 5% to 40% (see Tab. 1). A low macroscopic shear rate $\bar{\dot{\gamma}}$=8 s^{-1} was imposed in order to ensure that we are in the simplest case ('plastic' regime) where Eq. 5 is valid.

The sedimentation velocities $V(\phi)$ measured at a same macroscopic shear rate $\bar{\dot{\gamma}}$ are displayed in Fig. 9, rescaled by the velocity $V(\phi_0)$ measured for $\phi_0 = 5\%$. These values are compared to the dimensionless sedimentation velocity $V(\phi)/V(\phi_0)$ observed in viscous suspensions in the literature [13], which accounts for collective effects in Newtonian materials.

It is observed that the sedimentation velocity decreases very moderately with the volume fraction in a sheared yield stress fluid, whereas a strong decrease is observed in Newtonian fluids. E.g., at a 40% particle volume fraction, the sedimentation velocity in the sheared yield stress fluid decreases by only a factor

of 2 as compared to a 5% suspension, which is 4 times less important than in a Newtonian fluid.

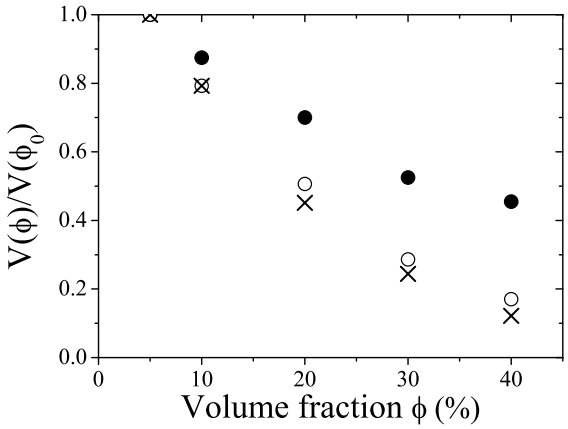

Figure 9: Dimensionless sedimentation velocity $V(\phi)/V(\phi_0)$ vs. particle volume fraction ϕ, where $\phi_0 = 5\%$, for suspensions sheared in a Couette geometry at a $\bar{\dot{\gamma}} = 8$ s^{-1} macroscopic shear rate (filled circles) and for viscous suspensions (crosses, data from [13]). We also plot the dimensionless velocity corrected for the impact of the volume fraction change on the apparent viscosity of the interstitial fluid (empty circles): $V(\phi)/V(\phi_0)\times\eta[\dot{\gamma}_l(\phi)]/\eta[\dot{\gamma}_l(\phi_0)]$, where $\eta[\dot{\gamma}_l(\phi)]$ is the apparent viscosity of the sheared interstitial yield stress fluid at a local shear rate $\dot{\gamma}_l(\phi)$ computed following Eq. 9.

4.2. Theoretical analysis

This observation can be understood by analyzing the behavior of the material at the local scale. Indeed, as the particles are rigid, shear is more and more concentrated in the fluid between neighboring particles as the particles get closer. This implies that, at a given macroscopic shear rate $\bar{\dot{\gamma}}$, the local shear rate $\dot{\gamma}_l$ in the interstitial fluid is an increasing function of the particle volume fraction ϕ. Then, when ϕ is increased, the apparent viscosity $\tau(\dot{\gamma}_l)/\dot{\gamma}_l = \tau_y/\dot{\gamma}_l + \eta_{HB}/\dot{\gamma}_l^{1-n}$ of the interstitial fluid decreases, i.e. the viscous resistance to sedimentation decreases, which may explain why $V(\phi)/V(\phi_0)$ is higher in a sheared yield stress fluid than in a viscous fluid of constant viscosity.

The value of the average local shear rate $\bar{\dot{\gamma}}_l$ can be estimated as a function of the macroscopic shear rate $\bar{\dot{\gamma}}$ and of the particle volume fraction ϕ, by comparing the macroscopic properties of the suspension (elastic modulus $G'(\phi)$, yield stress $\tau_y(\phi)$, consistency $\eta_{HB}(\phi)$) and those of the suspending fluid ($G'(0)$, $\tau_y(0)$,

$\eta_{HB}(0)$) [30]. E.g., the elastic energy stored below the yield stress in the suspension at the macroscopic scale $G'(\phi)\bar{\dot{\gamma}}^2$ must match the elastic energy stored at the microscopic scale, which is stored in the interstitial fluid only and is $(1-\phi)G'(0)\bar{\dot{\gamma}}_l^2$. This implies that $\bar{\dot{\gamma}}_l(\phi) = \bar{\dot{\gamma}}\sqrt{g(\phi)/(1-\phi)}$ where $g(\phi) = G'(\phi)/G'(0)$ is the linear response of the material [15, 30, 31]. A classical expression for $g(\phi)$ is the Krieger-Dougherty law $g(\phi) = (1-\phi/\phi_{\text{div}})^{-2.5\phi_{\text{div}}}$, which is in agreement with the experimentally observed behavior [15] for monodisperse suspensions. For sheared suspensions of monodisperse spheres, a reliable value of $\phi_{\text{div}} = 60.5\%$ was recently measured at a local scale [20]. This finally means that the average local shear rate in the interstitial fluid can be estimated with no fitting parameter as $\bar{\dot{\gamma}}_l(\phi) = \bar{\dot{\gamma}}\sqrt{(1-\phi/\phi_{\text{div}})^{-2.5\phi_{\text{div}}}(1-\phi)^{-1}}$ with $\phi_{\text{div}} = 60.5\%$, in agreement with previous experimental data [15, 30, 31].

We thus propose to model the sedimentation velocity $V(\phi)$ of a suspension of volume fraction ϕ by taking into account the local viscosity $\eta[\bar{\dot{\gamma}}_l(\phi)]$ of the interstitial fluid into Eq. 5, and by multiplying this last equation, valid for a single sphere only, by the same "hindrance function" $f_{\text{Newt.}}(\phi)$ as in a Newtonian fluid to account for collective effects ($f_{\text{Newt.}}(\phi)$ is the sedimentation velocity of a Newtonian suspension rescaled by the Stokes velocity). This finally leads to the following set of equations:

$$V(\phi) = \alpha\frac{\Delta\rho g d^2}{\eta[\bar{\dot{\gamma}}_l(\phi)]}f_{\text{Newt.}}(\phi) \tag{8}$$

$$\text{where} \quad \bar{\dot{\gamma}}_l(\phi) = \bar{\dot{\gamma}}\sqrt{(1-\phi/\phi_{\text{div}})^{-2.5\phi_{\text{div}}}(1-\phi)^{-1}} \tag{9}$$

with $\phi_{\text{div}} = 60.5\%$, where $\eta(\dot{\gamma}) = \tau(\dot{\gamma})/\dot{\gamma}$ is the apparent viscosity of the pure yield stress fluid sheared at a $\dot{\gamma}$ shear rate. We recall that Eq. 8 is *a priori* valid at low and large Bi^{-1} values only, and that the drag constant α is expected to take different values in the 'plastic' and 'viscous' regimes, and to be close to the value $1/18$ observed in Newtonian materials in the 'plastic' regime (see Sec. 3.5). It is worth noting that there is no fitting parameter in Eqs. 8, 9.

In order to test this model, we report in Fig. 9 the values of $V(\phi)/V(\phi_0) \times \eta[\bar{\dot{\gamma}}_l(\phi)]/\eta[\bar{\dot{\gamma}}_l(\phi_0)]$, where $\phi_0 = 5\%$, which should be equal to the dimensionless sedimentation velocity of a Newtonian fluid $f_{\text{Newt.}}(\phi)/f_{\text{Newt.}}(\phi_0)$ from Eq. 8. A fair agreement is observed between our theoretical expression and the values $f_{\text{Newt.}}(\phi)/f_{\text{Newt.}}(\phi_0)$ measured in Newtonian suspensions [13].

5. Conclusion

We have addressed the question of the impact of a flow on the stability of coarse particles suspended in yield stress fluids. In contrast with previous investigation [12], we have observed that shear induces sedimentation of the particles in all the studied systems, which were stable at rest. It thus seems that any density-mismatched suspension of particles or bubbles [32] in a yield stress fluid will tend to become heterogeneous when it is transported. It makes it particularly important to model shear-induced sedimentation as a function of the characteristics of shear and of the material properties.

At low shear rate ('plastic regime', $Bi^{-1}= \eta_{_{HB}}\dot{\gamma}^n/\tau_y < 1$), we have proposed a quantitative prediction of the sedimentation velocity, which is in good agreement with our experimental observations. We have shown that shear-induced sedimentation can be modelled by considering that the interstitial fluid behaves like a viscous fluid – of viscosity equal to the apparent viscosity $\tau(\dot{\gamma})/\dot{\gamma}$ of the sheared fluid – in the direction orthogonal to shear. The sedimentation velocity of spherical particles in a sheared yield stress fluid can then be fairly predicted using Eq. 8, with a drag constant α close to that observed in Newtonian media. An increase of the particle volume fraction ϕ plays here two contradictory roles: it hinders settling, which is accounted for by the same hindrance function $f(\phi)$ as in Newtonian fluids, and it decreases the viscous resistance of the interstitial fluid because of shear concentration between the particles, which is accounted for by estimating the local shear rate in the interstitial yield stress fluid with Eq. 9 [15, 30].

At this stage, this modelling has been shown to be valid at proximity of the yield stress only. The existence of a 'viscous' regime ($Bi^{-1}>> 1$) where the scaling of Eq. 8 should remain valid is predicted theoretically, but we could not test it experimentally. Nevertheless, our results suggest that the drag constant α should be significantly higher (by a factor of 3 or more) in this regime than in the 'plastic' regime, which would result in high shear-induced sedimentation velocities. The behavior at high shear rates thus remains to be fully characterized and understood.

Appendix A. Impact of the shear rate heterogeneity

In the following, we study the possible impact of the shear rate heterogeneity on the spatial characteristics of shear-induced sedimentation.

Let us assume, consistently with our findings in the 'plastic' regime (Sec. 3.5), that particles situated at a given radial position r in the gap settle in the sheared

yield stress fluid as in a viscous medium of local viscosity $\eta(r) = \tau(r)/\dot{\gamma}(r)$, i.e. that the local sedimentation velocity is $V(r) \propto 1/\eta(r)$. It is thus assumed here that the local sedimentation velocity $V(r)$ of the suspension at a given position is independent of the sedimentation velocity in its surroundings. The theoretical volume fraction profile $\bar{\phi}(z,t)$ corresponding to the experimental conditions after a given time t of shear can then be easily computed by averaging the theoretical volume fraction profile $\phi(r,z,t)$ at a given vertical position z from $r = R_1 = 4.4$ cm to $R_2 = 5.3$ cm.

To do that, defining $z = h$ as the top of the suspension, we start at time $t = 0$ with a homogeneous suspension of volume fraction $\phi_0 = 5\%$, i.e., we write $\phi(r,z,t=0) = \phi_0\,\mathrm{H}(h-z)$ with H the Heaviside function ($\mathrm{H}(z) = 1$ if $z \geq 0$ and $\mathrm{H}(z) = 0$ if $z < 0$). After a time t of shear at a given macroscopic shear rate, the local volume fraction is then computed as $\phi(r,z,t) = \phi_0\,\mathrm{H}(h - V(r)t - z)$, with the local sedimentation velocity $V(r) \propto 1/\eta(r)$ calculated from the experimentally measured value of $\eta(r)$ (see Fig. 3b). The profile $\bar{\phi}(z,t)$ that should theoretically be measured in these conditions is then the average of $\phi(r,z,t)$ between the radial positions R_1 and R_2 (the measurement window has a constant extent in the azimuthal direction) and is $\bar{\phi}(z,t) = \frac{1}{R_2-R_1}\int_{R_1}^{R_2} \phi_0\,\mathrm{H}(h-V(r)t-z)\,\mathrm{d}r$. Such profiles are compared to experimental profiles in Fig. A.10.

There is strong discrepancy between what is expected from this first naïve analysis and the experimental measurements. Whereas the experimental profiles show a rather narrow front with no broadening in time, the sedimentation front of the theoretical profiles gets broader and broader in time. As the local apparent viscosity $\eta(r)$ of the sheared fluid typically varies by a factor of 2 in the measurement zone (see Fig. 3b), it is indeed easily understood that the front corresponding to $\phi = 5\%$ should move 2 times faster than the front corresponding to ϕ=0%, which is clearly not the case experimentally.

This suggests that collective effects are at play, which tend to stabilize the front at a given speed basically set by the average apparent viscosity. This point may not be a surprise. In a Newtonian fluid, it is actually known that sedimentation velocities are correlated in the horizontal plane over very long distances, of order $10d\phi^{-1/3}$ [28]. For the particles we use in our study, this lengthscale is of the order of 1 cm, i.e. of the order of the gap size (which is 1.9 cm). This may thus explain our observations.

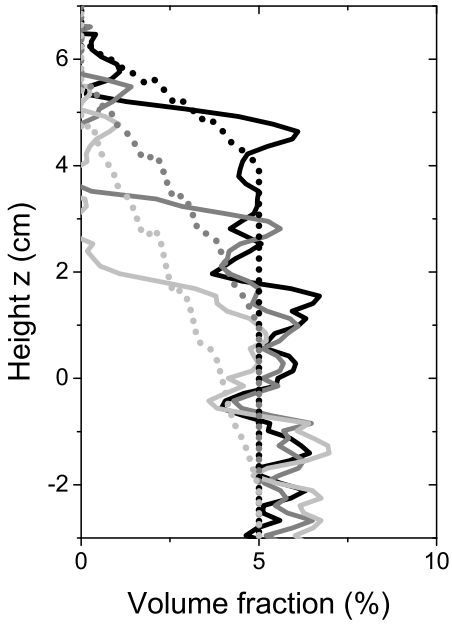

Figure A.10: Vertical volume fraction profiles observed in the gap of a Couette geometry in a 5% suspension of 275 μm glass beads in a concentrated emulsion of yield stress $\tau_y = 8.5$ Pa after 15 min (black line), 30 min (dark grey line) and 45 min (light grey line) of shear at $\bar{\dot{\gamma}} = 4\,\mathrm{s}^{-1}$. The dotted lines are the theoretical profiles expected from Eq. 5 by taking into account the heterogeneity of the apparent viscosity in the sheared material, under the assumption that the sedimentation velocity of the suspension at a given radial position is set by the local viscosity $\eta(r) = \tau(r)/\dot{\gamma}(r)$ of the sheared yield stress fluid only, independently of the sedimentation velocity in its surroundings.

Appendix B. Drag force exerted on a particle in a sheared yield stress fluid: theoretical analysis

We study the translational motion of a single particle of diameter d embedded in a sheared Herschel-Bulkley fluid. We focus on the case where translation of the particle is imposed at a constant velocity V in the direction $\underline{e}_3$ orthogonal to the plane ($\underline{e}_1$,$\underline{e}_2$) of shear. We try to compute the drag force F exerted by the fluid on the particle as a function of V, of the properties of the particle and of the fluid, and of the characteristics of shear.

In the studied problem, the particle occupies the domain Ω_p with boundary $\partial\Omega_p$ and the fluid occupies the domain Ω_f with boundary $\partial\Omega_f = \partial\Omega_p \cup \partial\Omega_\infty$. The fluid domain is sheared far from the particle at a given overall shear rate $\dot{\Gamma}$.

Then the velocity is prescribed on the external fluid domain boundary $\partial\Omega_\infty$

$$\underline{u} = \frac{1}{2}\dot{\Gamma}\left(x_2\underline{e}_1 + x_1\underline{e}_2\right) \tag{B.1}$$

The no-slip condition states that at the particle-fluid boundary $\partial\Omega_p$, the fluid velocity is that of the particle

$$\underline{u} = -V\underline{e}_3 \tag{B.2}$$

where V denotes the particle velocity (V is positive when the particle moves downward).

The isotropic tensorial form of the Herschel-Bulkley behavior law is

$$\begin{array}{ll} \boldsymbol{\tau} = 2\left[\left(\tau_y + \eta_{\text{HB}}\dot{\gamma}^n\right)/\dot{\gamma}\right]\boldsymbol{d} & \text{if } \boldsymbol{d} \neq 0 \\ 1/2\,\boldsymbol{\tau} : \boldsymbol{\tau} \leq \tau_y & \text{if } \boldsymbol{d} = 0 \end{array} \tag{B.3}$$

with $\boldsymbol{d}$ the strain rate tensor (i.e. the symmetric part of the velocity gradient) and $\boldsymbol{\tau}$ the deviatoric part of the Cauchy stress tensor. In Eq. B.3, the shear rate is $\dot{\gamma} = \sqrt{2\boldsymbol{d} : \boldsymbol{d}}$.

The boundary value problem for the motion of a single particle moving with velocity V in a sheared yield stress fluid is defined by Eqs. B.1, B.2, B.3, the no-body force momentum balance equation div $\boldsymbol{\sigma} = 0$ where $\boldsymbol{\sigma} = \boldsymbol{\tau} - p\boldsymbol{\delta}$ with p the pressure, and the incompressibility condition div $\underline{u} = 0$.

The drag force exerted by the yield stress fluid on the particle can be easily computed from the solution of Eqs. B.1 to B.3

$$\underline{F} = \mathrm{F}\underline{e}_z = \int_{\partial\Omega_p} \boldsymbol{\sigma}\cdot\underline{n}\,dS \tag{B.4}$$

with $\underline{n}$ the outward unit vector normal to the boundary of the particle.

An analytic solution of this problem is not available, it is thus not possible to compute F as a function of the material properties τ_y, η_{HB} and n, the particle diameter d and the loading parameters $\dot{\Gamma}$ and V. Leaving aside the possibility to solve numerically this problem, we restrict in the sequel to the situation of "slow" forced motion of the particle defined by $V \ll \dot{\Gamma}d$ (i.e., when the flow induced by the particle motion can be considered as a secondary flow as compared to the flow induced by shear). In these conditions, the solution of the problem defined by Eqs. B.1 to B.3 is looked for as an asymptotic expansion of the small dimensionless parameter $\varepsilon = V/\dot{\Gamma}d$. It is easily shown that, up to the second order in ε, the solution of this problem is

$$\underline{u} = \underline{u}_f + \varepsilon\underline{u}_{\text{p}} + O(\varepsilon^2) \tag{B.5}$$

and

$$p = p_f + \varepsilon p_{\mathrm{p}} + O(\varepsilon^2) \tag{B.6}$$

where $\underline{u}_f$ and p_f are the velocity and pressure in the sheared yield stress fluid when the particle is at rest, i.e. they are solutions of Eqs. B.1 to B.3 for $V = 0$, while $\underline{u}_{\mathrm{p}}$ and p_{p} are solutions of the boundary value problem

$$\begin{array}{rcll} \underline{u}_{\mathrm{p}} & = & v_{\mathrm{p}}\underline{e}_z & (\partial\Omega_p) \\ \underline{u}_{\mathrm{p}} & = & 0 & (\partial\Omega_\infty) \end{array} \tag{B.7}$$

with v_{p} defined as $v_{\mathrm{p}} = V/\varepsilon$. The Cauchy stress tensor is here $\boldsymbol{\sigma} = \boldsymbol{\sigma}_{\mathrm{f}} + \varepsilon\boldsymbol{\sigma}_{\mathrm{p}} + O(\varepsilon^2)$, with $\boldsymbol{\sigma}_{\mathrm{f}} = \boldsymbol{\tau}_f - p_f\boldsymbol{\delta}$ and $\boldsymbol{\sigma}_{\mathrm{p}} = \boldsymbol{\tau}_{\mathrm{p}} - p_{\mathrm{p}}\boldsymbol{\delta}$, where $\boldsymbol{\tau}_f$ and $\boldsymbol{\tau}_{\mathrm{p}}$ are the zeroth and first order term of an asymptotic expansion[4] $\boldsymbol{\tau} = \boldsymbol{\tau}_f + \varepsilon\boldsymbol{\tau}_{\mathrm{p}} + O(\varepsilon^2)$ of the constitutive law B.3 with respect to ε. Putting the strain rate tensor associated to the velocity field B.5 into Eq. B.3 yields

$$\boldsymbol{\tau}_{\mathrm{p}} = 2\left[\left(\tau_y + \eta_{\text{HB}}\dot{\gamma}_f^n\right)/\dot{\gamma}_f\right]\boldsymbol{d}_{\mathrm{p}} - 2\frac{\tau_y}{\dot{\gamma}_f}\frac{\boldsymbol{d}_f : \boldsymbol{d}_{\mathrm{p}}}{\boldsymbol{d}_f : \boldsymbol{d}_f}\boldsymbol{d}_f + 2\eta_{\text{HB}}(n-1)\dot{\gamma}_f^{n-1}\frac{\boldsymbol{d}_f : \boldsymbol{d}_{\mathrm{p}}}{\boldsymbol{d}_f : \boldsymbol{d}_f}\boldsymbol{d}_f \tag{B.8}$$

where $\boldsymbol{d}_f$ and $\dot{\gamma}_f = \sqrt{2\boldsymbol{d}_f : \boldsymbol{d}_f}$ are the strain rate tensor and the shear rate associated to $\underline{u}_f$ while $\boldsymbol{d}_{\mathrm{p}}$ is the strain rate tensor associated to $\underline{u}_{\mathrm{p}}$. Eq. B.8 is valid only if the fluid deforms ($\dot{\gamma}_f \neq 0$) everywhere in the fluid domain. Such an assumption is undoubtedly fulfilled here because in the zeroth order problem, the fluid domain is uniformly sheared on its outside boundary (see Eq. B.1).

When the particle is at rest, the symmetries of the problem imply that the net force $\int_{\partial\Omega_p} \boldsymbol{\sigma}_{\mathrm{f}} \cdot \underline{n}\, dS$ exerted by the fluid on the particle is zero. When the particle moves slowly (i.e. $\varepsilon \ll 1$), the drag force is thus a first order quantity in ε

$$\underline{F} = \mathrm{F}\underline{e}_z = \varepsilon \int_{\partial\Omega_p} \boldsymbol{\sigma}_{\mathrm{p}} \cdot \underline{n}\, dS + O(\varepsilon^2) \tag{B.9}$$

Let us point out that for orthogonal flows, i.e. when $\boldsymbol{d}_f : \boldsymbol{d}_{\mathrm{p}} = 0$, Eq. B.8 reduces to $\boldsymbol{\tau}_{\mathrm{p}} = 2\left[\left(\tau_y + \eta_{\text{HB}}\dot{\gamma}_f^n\right)/\dot{\gamma}_f\right]\boldsymbol{d}_{\mathrm{p}}$, which corresponds to a Newtonian behavior, thus justifying the use of expressions valid for Newtonian materials such as Eq. 5. Of course, around a spherical particle, $\boldsymbol{d}_f : \boldsymbol{d}_{\mathrm{p}} \neq 0$ and things are more complex. Because the shear tensor field (Eq. B.8) is then a nonlinear function

[4]Note that this approach is similar to that used in hydrodynamic stability analysis, where linearization of the stress field is performed when adding a perturbation to a base flow [33].

of both the zeroth and first order problem solutions, it is actually not possible to predict even qualitatively how the force F depends upon quantities $\dot{\Gamma}$ and V in a general case. Nevertheless some results can be obtained in the 'plastic' and 'viscous' regimes defined respectively by $Bi^{-1} \ll 1$ and $Bi^{-1} \gg 1$ where the inverse Bingham number is $Bi^{-1} = \eta_{HB}\dot{\Gamma}^n/\tau_y$.

Plastic regime

In the 'plastic' regime ($\tau_y \gg \eta_{HB}\dot{\gamma}^n$), if $\boldsymbol{d}_f \neq 0$, the asymptotic expansion of the Herschel-Bulkley law is

$$\boldsymbol{\tau} = 2\tau_y/\dot{\gamma}_f\, \boldsymbol{d}_f + \varepsilon \left(2\tau_y/\dot{\gamma}_f \boldsymbol{d}_{\mathrm{p}} - 2\frac{\tau_y}{\dot{\gamma}_f}\frac{\boldsymbol{d}_f : \boldsymbol{d}_{\mathrm{p}}}{\boldsymbol{d}_f : \boldsymbol{d}_f}\boldsymbol{d}_f \right) \tag{B.10}$$

The leading term of Eq. B.10 corresponds to a rigid plastic constitutive law, and the zeroth order problem solution is the velocity field of a perfect rigid-plastic material strained at a constant shear rate $\dot{\Gamma}$ flowing around a particle rotating freely around a fixed point. If $(\underline{v}_1, p_1)$ denotes the solution of this problem for $\dot{\Gamma} = 1$, a classic result of the theory of plasticity [34] asserts that the solution of the problem is $\underline{u}_f = \dot{\Gamma}\underline{v}_1$, $p_f = p_1$ for any value of $\dot{\Gamma}$.

Putting this result into Eq. B.10 yields the first order constitutive law

$$\boldsymbol{\tau}_{\mathrm{p}} = 2\tau_y/\dot{\gamma}_f \left(\boldsymbol{d}_{\mathrm{p}} - \frac{\boldsymbol{d}_1 : \boldsymbol{d}_{\mathrm{p}}}{\boldsymbol{d}_1 : \boldsymbol{d}_1}\boldsymbol{d}_1 \right) \tag{B.11}$$

with $\boldsymbol{d}_1$ the strain rate tensor associated to $\underline{v}_1$.

The first order constitutive law being linear, so is the first order problem. Thus both $\boldsymbol{\tau}_{\mathrm{p}}$ and p_{p} depend linearly upon v_{p}. It is sufficient to report this property into Eq. B.9 to show that the drag force is a linear function of the quantity $\tau_y/\dot{\Gamma} \times Vd$. Then we do have

$$\text{If} \quad \frac{\eta_{\mathrm{HB}}\dot{\Gamma}^n}{\tau_y} \ll 1 \quad \text{and} \quad \frac{V}{\dot{\Gamma}d} \ll 1 \quad \text{then} \quad \mathrm{F} \propto V\frac{\tau_y}{\dot{\Gamma}}d \tag{B.12}$$

These equations applied in the case of sedimentation, where the driving force is $\mathrm{F} \propto \Delta\rho g d^3$, yield

$$V \propto \frac{\Delta\rho g d^2}{\tau_y/\dot{\Gamma}} \tag{B.13}$$

Viscous regime

We now turn to the situation where the viscous stress $\eta_{\text{HB}}\dot{\Gamma}^n$ is much larger than the yield stress τ_y; the asymptotic expansion of the Herschel-Bulkley law is then

$$\boldsymbol{\tau} = 2\eta_{\text{HB}}\dot{\gamma}_f^{n-1}\boldsymbol{d}_f + \varepsilon\left(2\eta_{\text{HB}}\dot{\gamma}_f^{n-1}\boldsymbol{d}_{\text{p}} + 2(n-1)\eta_{\text{HB}}\dot{\gamma}_f^{n-1}\frac{\boldsymbol{d}_f : \boldsymbol{d}_{\text{p}}}{\boldsymbol{d}_f : \boldsymbol{d}_f}\boldsymbol{d}_f\right) \tag{B.14}$$

In this situation, the leading term of Eq. B.10 corresponds to a power law material. Then, it is easily shown that the zeroth order solution of the problem is ($\underline{u}_f = \dot{\Gamma}\underline{v}_1$, $p_f = \dot{\Gamma}^n p_1$) for any value of $\dot{\Gamma}$ with ($\underline{v}_1, p_1$) the solution of the first order problem for $\dot{\Gamma} = 1$. Thus, performing similar computations as in the 'plastic' regime, and putting this result into the first order term of the asymptotic expansion of the constitutive law yields the linear law

$$\boldsymbol{\tau}_{\text{p}} = 2\eta_{\text{HB}}\dot{\gamma}_f^{n-1}\left(\boldsymbol{d}_{\text{p}} + (n-1)\frac{\boldsymbol{d}_1 : \boldsymbol{d}_{\text{p}}}{\boldsymbol{d}_1 : \boldsymbol{d}_1}\boldsymbol{d}_1\right) \tag{B.15}$$

Therefore, we do again obtain a linear first order problem, which implies that both $\boldsymbol{\tau}_{\text{p}}$ and p_{p} depend linearly upon $V \times \dot{\Gamma}^{n-1}$. Finally, in the 'viscous' regime the drag force is given by

$$\text{If} \quad \frac{\eta_{\text{HB}}\dot{\Gamma}^n}{\tau_y} \gg 1 \quad \text{and} \quad \frac{V}{\dot{\Gamma}d} \ll 1 \quad \text{then} \quad \text{F} \propto V\,\eta_{\text{HB}}\dot{\Gamma}^{n-1}d \tag{B.16}$$

These equations applied in the case of sedimentation, where the driving force is $\text{F} \propto \Delta\rho g d^3$, yield

$$V \propto \frac{\Delta\rho g d^2}{\eta_{\text{HB}}\dot{\Gamma}^{n-1}} \tag{B.17}$$

References

[1] A.R. Oroskar, R.M. Turian, The critical velocity in pipeline flow of slurries, AIChE J. 26 (1980) 550-558.

[2] J.T. Davies, Calculation of critical velocities to maintain solids in suspension in horizontal pipes, Chem. Eng. Sci. 42 (1987) 1667-1670.

[3] D. Leighton, A. Acrivos, Viscous resuspension, Chem. Eng. Sci. 41 (1986) 1377-1384.

[4] K. Zhang, A. Acrivos, Viscous resuspension in fully developed laminar pipe flows, Int. J. Multiphase Flow 20 (1994) 579-591.

[5] N. Roussel, A theoretical frame to study stability of fresh concrete, Mater. Struct. 39 (2006) 75-83.

[6] N. Roussel (Ed.), Understanding the Rheology of Concrete, Woodhead Publishing, Cambridge, 2011.

[7] A.N. Beris, J.A. Tsamopoulos, R.C. Armstrong, R.A. Brown, Creeping motion of a sphere through a Bingham plastic, J. Fluid Mech. 158 (1985) 219-244.

[8] H. Tabuteau, P. Coussot, J.R. de Bruyn, Drag force on a sphere in steady motion through a yield-stress fluid, J. Rheol. 51 (2007) 125-137.

[9] R. Cooke, Laminar flow settling: the potential for unexpected problems, Proc. 15th International Symposium on Hydrotransport, Banff, Canada 2002.

[10] R.P. Chhabra, Bubbles, Drops, and Particles in Non-Newtonian Fluids, second ed., Taylor & Francis, Boca Raton, 2006.

[11] G. Gheissary, B.H.A.A. vandenBrule, Unexpected phenomena observed in particle settling in non-Newtonian media, J. Non-Newtonian Fluid Mech. 67 (1996) 1-18.

[12] O. Merkak, L. Jossic, A. Magnin, Migration and sedimentation of spherical particles in a yield stress fluid flowing in a horizontal cylindrical pipe, AIChE J. 55 (2009) 2515-2525.

[13] T.J. Hanratty, A. Bandukwala, Fluidization and sedimentation of spherical particles, AIChE J. 3 (1957) 293-296.

[14] R.H. Davis, A. Acrivos, Sedimentation of noncolloidal particles at low Reynolds-numbers, Annu. Rev. Fluid Mech. 17 (1985) 91-118.

[15] F. Mahaut, X. Chateau, P. Coussot, G. Ovarlez, Yield stress and elastic modulus of suspensions of noncolloidal particles in yield stress fluids, J. Rheol. 52 (2008) 287-313.

[16] G. Ovarlez, S. Rodts, A. Ragouilliaux, P. Coussot, J. Goyon, and A. Colin, Wide-gap Couette flows of dense emulsions: Local concentration measurements, and comparison between macroscopic and local constitutive law measurements through magnetic resonance imaging, Phys. Rev. E 78 (2008) 036307.

[17] P. Coussot, L. Tocquer, C. Lanos, G. Ovarlez, Macroscopic vs local rheology of yield stress fluids, J. Non-Newtonian Fluid Mech. 158 (2009) 85-90.

[18] J.S. Raynaud, P. Moucheront, J.C. Baudez, F. Bertrand, J.P. Guilbaud, P. Coussot, Direct determination by NMR of the thixotropic and yielding behavior of suspensions, J. Rheol. 46 (2002) 709-732.

[19] S. Rodts, F. Bertrand, S. Jarny, P. Poullain, P. Moucheront, Développements récents dans l'application de l'IRM à la rhéologie et à la mécanique des fluides, C. R. Chim. 7 (2004) 275-282.

[20] G. Ovarlez, F. Bertrand, S. Rodts, Local determination of the constitutive law of a dense suspension of noncolloidal particles through MRI, J. Rheol. 50 (2006) 259-292.

[21] G. Ovarlez, S. Rodts, X. Chateau, P. Coussot, Phenomenology and physical origin of shear-localization and shear-banding in complex fluids, Rheol. Acta 48 (2009) 831-844.

[22] J.G. Oldroyd, On the Formulation of Rheological Equations of State, Proc. R. Soc. London Ser. A 200 (1950) 523-541.

[23] P. Coussot, Rheometry of Pastes, Suspensions and Granular Materials, John Wiley & Sons, Hoboken, 2005.

[24] G. Ovarlez, Q. Barral, P. Coussot, Three dimensional jamming and flows of soft glassy materials, Nat. Mater. 9 (2010) 115-119.

[25] B. Rabideau, P. Moucheront, F. Bertrand, S. Rodts, N. Roussel, C. Lanos, and P. Coussot, The extrusion of a model yield stress fluid imaged by MRI velocimetry, J. Non-Newtonian Fluid Mech. 165 (2010) 394-408.

[26] J.M. Piau, Carbopol gels: Elastoviscoplastic and slippery glasses made of individual swollen sponges: Meso- and macroscopic properties, constitutive equations and scaling laws, J. Non-Newtonian Fluid Mech. 144 (2007) 1-29.

[27] C.W.J. Beenakker, P. Mazur, Is Sedimentation container-shape dependent?, Phys. Fluids 28 (1985) 3203-3206.

[28] E. Guazzelli, J. Hinch, Fluctuations and Instability in Sedimentation, Annu. Rev. Fluid Mech. 43 (2011) 97-116.

[29] M.P. Brenner, Screening mechanisms in sedimentation, Phys. Fluids 11 (1999) 754-772.

[30] X. Chateau, G. Ovarlez, K. Luu Trung, Homogenization approach to the behavior of suspensions of noncolloidal particles in yield stress fluids, J. Rheol. 52 (2008) 489-506.

[31] T.-S. Vu, G. Ovarlez, X. Chateau, Macroscopic behavior of bidisperse suspensions of noncolloidal particles in yield stress fluids, J. Rheol. 54 (2010) 815-833.

[32] J. Goyon, F. Bertrand, O. Pitois, G. Ovarlez, Shear Induced Drainage in Foamy Yield-Stress Fluids, Phys. Rev. Lett. 104 (2010) 128301.

[33] C. Nouar, A. Bottaro, J. P. Brancher, Delaying transition to turbulence in channel flow: revisiting the stability of shear-thinning fluids, J. Fluid. Mech. 592, 177-194 (2007).

[34] R. Hill, The mathematical theory of plasticity, Clarendon Press, Oxford and New York, 1998.